Relationship of *XIST* Expression and Responses of Ovarian Cancer to Chemotherapy[1]

Kuan-Chun Huang, Pulivarthi H. Rao, Ching C. Lau, Edith Heard, Shu-Kay Ng, Carolyn Brown, Samuel C. Mok, Ross S. Berkowitz, and Shu-Wing Ng[2]

Laboratory of Gynecologic Oncology, Department of Obstetrics and Gynecology, Brigham and Women's Hospital and Harvard Medical School, Boston, Massachusetts 02115 [K-C. H., S. C. M., R. S. B., S-W. N.]; Baylor College of Medicine, Texas Children's Cancer Center, Houston, Texas 77030 [P. H. R., C. C. L.]; CNRS, Institut Curie-Recherche, 75248 Paris, France [E. H.]; Centre of Statistics, Department of Mathematics, University of Queensland, St. Lucia, Brisbane, QLD 4072, Australia [S-K. N.]; and Department of Medical Genetics, University of British Columbia, Vancouver, British Columbia, V6T 1Z3, Canada [C. B.]

Abstract
Expression profiling to characterize cancer pharmacology has become a new approach to discover novel molecular targets for prognostic markers and cancer therapy. In a study to compare the global RNA expression profiles between primary and recurrent ovarian tumors from the same patient, we have identified *XIST* (inactive X chromosome-specific transcripts) as the most differentially expressed gene that was down-regulated in the recurrent tumor. *XIST* encodes a spliced noncoding polyadenylated transcript that is unique in being expressed exclusively from the inactive X chromosome and is involved in the X-inactivation process. Subsequent characterization of *XIST* expression in a panel of female cancer cell lines showed that the expression level of *XIST* correlates significantly with Taxol sensitivity. The clinical relevance of this observation is demonstrated by the strong association between *XIST* RNA levels and disease-free periods of ovarian cancer patients in a group of 21 ovarian cancer cases with Taxol in the therapeutic regiments. Cytogenetic studies on ovarian cancer cell lines indicated that loss of inactive X chromosome is one mechanism for the loss of *XIST* transcripts in the cell lines. Our data suggest that *XIST* expression may be a potential marker for chemotherapeutic responses in ovarian cancer.

Introduction
Currently, clinical management of epithelial ovarian cancers is surgical cytoreduction followed by consolidative chemotherapy. First-line chemotherapy in ovarian cancer consists of a platinum analogue in combination with Taxol (1). Despite a significant initial response rate of advanced ovarian carcinoma to the first-line chemotherapy, many patients relapse, and fewer than 15% of the patients will become long-term survivors (2), suggesting an intrinsic or acquired resistance to first-line chemotherapy in ovarian cancer. However, the molecular basis for chemoresistance and the development of recurrence in ovarian carcinoma is still largely unknown.

Currently, cDNA microarray technology has been used as a new approach to characterize cancer pharmacology (3, 4) and to predict clinical outcome (5–7). We initiated a study of comparing the global transcription profiles between primary and recurrent ovarian tumors of the same patient. In one such analysis of a recurrent tumor (RC680) salvaged from ascitic fluid and the paired primary tumor (PC598C) of the same patient, the gene with the highest differential expression in these two RNA populations was *XIST*.[3] Early in mammalian embryogenesis, X chromosome inactivation leads to the *cis*-limited transcriptional silencing of most of the genes on one of the two X chromosomes in female somatic cells, resulting in dosage compensation between males and females (8). Classical genetic studies have defined the X inactivation center at Xq13, from which X inactivation initiates and spreads along the X chromosome (9). The inactive X chromosome is heterochromatic, late-replicating in S-phase, underacetylated at histones H3 and H4, and highly methylated at some regions (10). The *XIST* gene resides within the X inactivation center and is the only transcript expressed exclusively from the inactive X chromosome (11). In female ES cells prior to X inactivation, low-level *XIST* expression can be detected from both active X chromosomes. After differentiation, *XIST* is expressed at high levels only from the inactive X chromosome through stabilization of *XIST* transcripts at the inactive X chromosome (12). Targeted mutation of the *XIST* homologue in mouse (*Xist*) indicates that the *Xist* RNA is required for female dosage compensation (13, 14) and *XIST* YAC transgenic experiments have also demonstrated that *XIST* is both necessary and sufficient for X inactivation (15). Clinically, the severe phenotype of Turner syndrome has been associated with small ring X chromosome, where the *XSIT* locus is either not present or not expressed. It has been hypothesized that the loss of *XIST* results in functional disomy for the genes contained in the ring (16).

The cell lines derived from RC680, OVCA680, and 15 other ovarian cancer cell lines were tested for sensitivity to anticancer drugs including carboplatin and Taxol, which the

[3] The abbreviations used are: *XIST*, inactive X chromosome-specific transcripts; YAC, yeast artificial chromosome; FISH, fluorescence *in situ* hybridization; DAPI, 4′,6-diamidino-2-phenylindole; SKY, spectral karyotyping; ES, embryonic stem cell; XIAP, X-linked inhibitor of apoptosis.

patient had received. Statistical analysis showed a significant association between Taxol sensitivity and *XIST* RNA level. Neither carboplatin nor cisplatin showed such correlation. Cytogenetic studies of the cell lines by spectral karyotyping, RNA FISH, and combined immunostaining and chromosome painting have suggested that loss of inactive X chromosome is one mechanism for the loss of *XIST* expression in some cell lines. To estimate the clinical significance of *XIST* expression, 21 cases of ovarian carcinoma tissues from the patients who were treated with Taxol and platinum drug were investigated, and *XIST* expression was found to be strongly associated with the patient responses to chemotherapy. Our data suggest that *XIST* is a potential marker for chemoresponse prediction in ovarian cancer.

Materials and Methods

cDNA Microarray Analysis. Total RNA was extracted from the primary and recurrent tumor cells by Trizol reagent (Invitrogen Life Technologies, Inc.). Poly(A) RNA was purified from total RNA by Oligotex mRNA kit (Qiagen). RNA concentration was determined by a RiboGreen fluorescence method (Molecular Probe). cDNA synthesis and microarray hybridization was performed by GenomeSystems, Inc. through a subcontract to the Center for Genomics Research of Harvard University. Hybridization was performed on a UniGEM V microarray from Incyte Pharmaceuticals, Inc., which contains 7000 sequence-verified human genes and expressed sequence tag sequences mapped to National Center for Biotechnology Information's UniGene database.

Cell Lines and Tumor Samples. Sixteen ovarian cancer cell lines were used in this study. ALST, CAOV3, OVCA3, OVCA420, OVCA429, OVCA432, OVCA433, OVCA633, OVCA680, OVCA702, and OVCA810 were established in our laboratory from tumor tissues obtained from different patients. OVCA680 and OVCA702 were derived from recurrent ovarian carcinomas, whereas others were all derived from primary ovarian carcinoma tissues. SKOV3, ES-2, and TOV21G were purchased from American Tissue Culture Collection. RMG-1 and RMUG-L were purchased from Japanese Collection of Research Bioresources (JCRB Cell Bank). ES-2 was maintained in McCoy's SA medium supplemented with 10% FCS, whereas RMG-1 and RMUG-L were cultured with DMEM-F12 HAM medium plus 10% FCS. Other ovarian cancer cell lines were grown in medium 199 and MCDB 105 (1:1) supplemented with 10% FCS. Five breast cancer cell lines used in our study were MDA-MB231, MDA-MB361, MDA-MB453, MDA-MB468, and MCF-7. All breast cancer cell lines were obtained from American Tissue Culture Collection and maintained in DMEM supplemented with 10% FCS. Ovarian tumors were obtained from patients at Brigham and Women's Hospital in Boston. All of the surgical specimens were collected with patient consents and were confirmed by histological examination.

Quantitative Real-Time PCR Analysis. TaqMan Reverse Transcription reagents (ABI) were applied for cDNA synthesis. The SYBR Green reagents kit (ABI) was used for quantitative real-time PCR analysis and performed according to the manufacturer's recommendation. During PCR, reactions were continuously monitored by an ABI Prism 5700 Sequence Detector (ABI). Cyclophilin messages were used as the internal control. The sequences of the primers used were listed as follows: XIST-11302F, 5′-GCAGTTTGCCCTAC-TAGCTCCT-3′; XIST-11456R, 5′-TCCTCAGGTCTCACAT-GCTCA-3′; Cyc-531F, 5′-GATGCTCCTGCGTTCTGATGT-3′; and Cyc-631R, 5′-GGTGGAAGCTGCTTCCCTTAA-3′. All primers were designed with PrimerExpress 1.5 software (ABI). All of the forward and reverse primers were designed on different exons separated by long introns to prevent noise signals generated from contaminated genomic DNA during the PCR reactions.

Drug Toxicity Assay. Drug cytotoxicity was determined by MTT dye-based methodology. Briefly, cells were seeded in 100 μl of medium (5000 cells) per well in 96-well plates. After overnight incubation, 100 μl of medium with different dilutions of Taxol were prepared and added to treat the cells for 48 h. Cell viability was quantified with the MTT cell proliferation assay kit (Roche) as described by the manufacturer's manual. The IC$_{50}$ is the concentration of drug resulting in a 50% reduction in absorbance at 550 nm to that of untreated cells. Every assay was performed in triplicates, and the drug IC$_{50}$ of each cell line was the average of three to six independent experiments.

Statistical Analysis. Correlation analysis of the relationship between *XIST* RNA level and the drug IC$_{50}$ (or relapse time) was carried out using the MINITAB statistical package. The Pearson correlation coefficient calculated between any two variables provides a measure of the strength of their linear relationship. Its significance is tested using a two-tailed *t* test. Both the calculation of the Pearson correlation coefficient and its test are based on two assumptions: (*a*) each pair of observations is independent of any other pair; and (*b*) each variable is normally distributed. In view of the second assumption, log transformation is therefore applied for each variable for the statistical analysis. For comparison, we provide *P*s obtained using Efron's (17) nonparametric bootstrap resampling method. To examine the clinical relevance of *XIST* expression in responses to cancer chemotherapy, multiple regression analysis was carried out using the MINITAB package. The three subtypes (serous, mucinous, and endometrioid) in the histology information was transformed into two dummy variables, whereas a binary (0, 1) variable was adopted for the stage by combining stages 3, 3C, and 4 into one group and stages 1A and 2A into the other. In addition, the relapse time, CA125, and age were transformed into log form. We adopted backwards elimination steps to select predictor variables. The method started with all variables in the regression equation. Then the variable was removed one by one, based on the *F*s associated with the variables. The procedure was terminated when no variable in the regression equation had an *F* that was <4. Residual plots were used to check the adequacy of the final model.

Combined Immunostaining and Chromosome Painting. Cultures were synchronized by 260 nM demecolcine (Sigma) for 18–24 h, and metaphase cells were differentially collected by mitotic shake-off method. Metaphase spreads were prepared as described before (18). After removing excess liquid, the slide was always kept in a humidified chamber for both immunolabeling and DNA FISH processes. For

Fig. 1. Microarray analysis of RNA prepared from paired primary ovarian tumor (*X-axis*) *versus* recurrent tumor (*Y-axis*). The relative intensities of signals generated by the Cy3- and Cy5-probes are shown. Each *blue spot* represents an individual gene on the microarray, whereas the *red spots* are signals from controls designed by the company. The signals are clustered in panels according to the folds of difference of intensities. Genes whose expressions are up-regulated in the recurrent tumors are clustered in the positive panels, whereas genes whose expressions are down-regulated are clustered in the negative panels. The *XIST* data point was indicated in the graph.
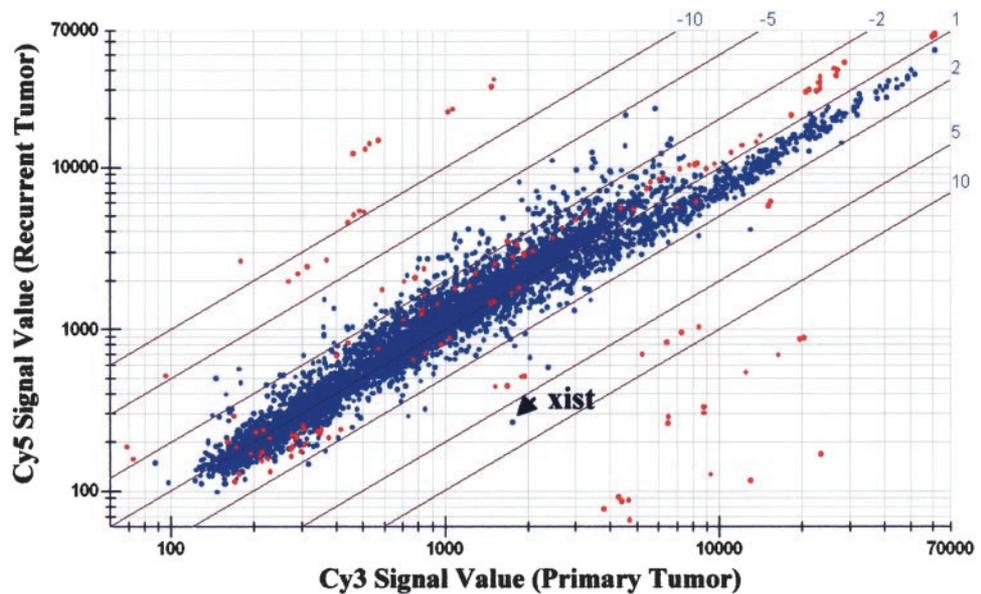
immunostaining of acetylated histone H4, the slide was blocked with 40 μl of 3% donkey serum in KCM buffer (18) for 30 min and followed by 40 μl of anti-acetylhistone H4 (Lys12; Upstate Biotechnology) antibody (1:90) incubation for 1 h. Then the slide was washed twice at room temperature for 5 min each with KCM buffer. Biotin-conjugated donkey anti-rabbit secondary antibody (Pierce) was used at $\times$200 dilution as described for the primary antibody. After the final wash, the slide was fixed in 3:1 methanol/acetic acid (v/v) for 10 min at room temperature and allowed to air dry. The slide was then processed for DNA FISH. The chromosomes on the slide were denatured by applying 100 μl of denaturing solution (0.5 N NaOH, 1.5 M NaCl) for 5 min at room temperature, followed by neutralization solution [0.5 M Tris-HCl (pH 7.4), and 1.5 M NaCl] for 5 min at room temperature twice. The slide then was prepared, hybridized to FITC-labeled X chromosome paint probe (Vysis, Inc.), and washed as described in the manufacturer's manual. The biotinylated anti-rabbit antibody was detected using Texas Red conjugated Streptavidin (Pierce) diluted 200 times in 4 $\times$ SSC (pH 7.2)/1% BSA at room temperature for 1 h in the dark. The slide was washed twice at room temperature for 5 min each with 4$\times$ SSC (pH 7.2)/0.1% Tween 20, followed by standard mounting protocol with Vectashield mounting medium, which contains DAPI as the counterstain (Vector Lab). The image was captured by an Olympus BX60 fluorescence microscope equipped with an Optronics CCD camera.

RNA FISH. Interphase nuclei were prepared, and RNA FISH was performed as described before (15). The human *XIST* probe was a pool of ~3.5 kb of sequence derived from exon 1 and 1 kb derived from exon 6 (15).

SKY. Metaphase spreads were prepared and hybridized with a mixture of 24 differentially labeled chromosome painting probes according to the manufacturer's recommendation (Applied Spectral Imaging, Inc.). The images were captured with an ASI camera and analyzed with SkyView 1.2 software (Applied Spectral Imaging, Inc.).

Results

A cDNA microarray analysis of RNA samples prepared from paired primary and recurrent ovarian tumor cells was performed as described in "Materials and Methods" (Fig. 1). The gene *XIST* was found to be the most differentially expressed and down-regulated gene in the recurrent tumor (6.7-fold by microarray analysis and 51.3-fold by real-time quantitative PCR). We established a cell line, named OVCA680, from the recurrent tumor. This and 15 other ovarian carcinoma cell lines were subjected to drug sensitivity assays with a panel of antineoplastic agents. Because the patient from whom the tumor specimens were obtained has been treated with Taxol and platinum drug during the first-line chemotherapy, we focused on these two types of anti-cancer agents (Table 1). Compared with other cell lines, OVCA680 demonstrated a high level of Taxol resistance and moderate resistance to carboplatin and cisplatin. We also determined the relative levels of *XIST* transcripts in the cell lines by quantitative real-time PCR (Table 1). Similar to other microarray studies (3, 4), a natural logarithm was applied to normalize the data as described in "Materials and Methods." Significant correlation was found between the levels of *XIST* transcript and Taxol IC_{50}s ($r = -0.584$; Fig. 2*a, solid regression line*). Using a two-tailed *t* test, the *P* is 0.018. For comparison, we calculated the *P* from 1000 bootstrap samples for the null hypothesis of zero correlation, $P_{boot} = 0.016$. However, the levels of *XIST* transcript is not significantly correlated with carboplatin ($r = 0.017$; $P = 0.949$, $P_{boot} = 0.946$; Fig. 2*b*) and cisplatin ($r = 0.116$; $P = 0.668$, $P_{boot} = 0.670$; Fig. 2*c*). Because carboplatin and cisplatin involve similar mechanisms of cell killing, the IC_{50}s of these two drugs exhibit strong correlation ($r = 0.892$; $P < 0.001$, $P_{boot} < 0.001$). The regression analysis of *XIST* expression to Taxol IC_{50}s showed an inverse correlation, whereas there was no significant correlation to both carboplatin IC_{50} and cisplatin IC_{50}s. When we included the results of five breast cancer cell

Table 1   XIST expression and drug IC$_{50}$ in a panel of ovarian cancer cell lines.

Relative *XIST* expression levels and IC$_{50}$ for Taxol, carboplatin, and cisplatin in various ovarian cancer cell lines.

| Cell line	Subtype	Ln(XIST)[a]	Ln(Taxol IC$_{50}$)[b]	Ln(Carboplatin IC$_{50}$)[b]	Ln(Cisplatin IC$_{50}$)[b]
SKOV3	Serous	9.58	−21.05	−9.95	−11.37
CAOV3	Serous	−2.30	−9.41	−9.99	−11.75
OVCA3	Serous	1.51	−9.31	−9.49	−11.42
ALST	Serous	0.31	−8.57	−7.16	−9.88
OVCA420	Serous	11.70	−9.21	−8.59	−10.16
OVCA429	Serous	11.05	−17.47	−7.23	−8.98
OVCA432	Serous	2.60	−9.57	−0.04	−11.01
OVCA433	Serous	9.73	−9.23	−7.69	−9.41
OVCA633	Serous	−2.30	−9.22	−7.11	−9.00
OVCA680	Serous	2.65	−9.21	−8.05	−10.91
OVCA702	Serous	8.36	−14.21	−8.01	−9.69
OVCA810	Clear	2.55	−8.42	−6.94	−8.29
ES-2	Clear	10.44	−23.29	−9.72	−11.20
RMG1	Clear	−2.30	−12.28	−8.78	−10.55
TOV21G	Clear	0.00	−8.68	−9.73	−11.01
RMUG-L	Mucinous	1.91	−11.71	−8.36	−9.19

[a] XIST RNA level is presented as a natural logarithm of the expression level relative to that of TOV21G.
[b] IC$_{50}$ is presented as a natural logarithm of actual value in the unit of M.
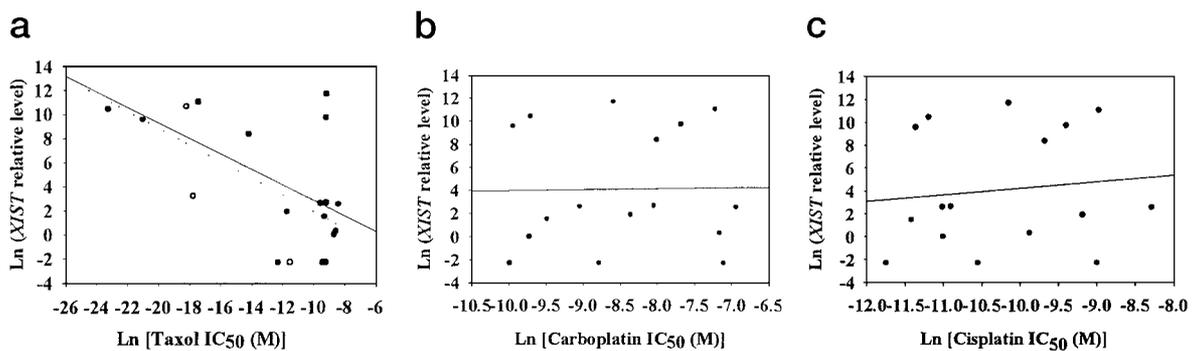
Fig. 2.   a, XIST expression levels and Taxol IC$_{50}$s of 16 ovarian and 5 breast cancer cell lines are plotted. The data points for ovarian cancer cell lines are presented as ●, and data points for breast cancer cell lines are presented as ○. Both variables (expression level and IC$_{50}$) are natural log-transformed. The regression lines are also shown in the graph. The *solid regression line* is calculated from ovarian cancer cell line data only, and the *dotted line* is plotted using combined data from ovarian and breast cancer cell lines. The five breast cancer cell lines used in this study were MDA-MB231, MDA-MB361, MDA-MB453, MDA-MB468, and MCF-7. *b, XIST* expression levels and carboplatin IC$_{50}$s of 16 ovarian cancer cell lines are plotted. The regression line is shown in the graph (*c*); *XIST* expression levels and cisplatin IC$_{50}$s of 16 ovarian cancer cell lines are plotted. The regression line is shown in the graph.

lines in the correlation analysis of Taxol IC$_{50}$ and *XIST* expression level, we obtained an even more significant correlation ($r = −0.601$; $P = 0.004$, $P_{boot} = 0.004$; Fig. 2*a, dotted regression line*).

To investigate the mechanism(s) by which *XIST* expression is regulated, several cytogenetic experiments were performed. SKY analysis of the cell lines showed extensive translocation and only one X chromosome in the OVCA680 cells (Fig. 3*a*). Because histone underacetylation is one of the hallmarks unique to inactive X chromosome, we performed a combined immunostaining and X chromosome painting experiment on the metaphase spreads of OVCA680 cells to determine the histone acetylation status of the single X chromosome. A strong signal for acetylated histone H4 was observed on the X chromosome (Fig. 3, *b* and *c*), indicating that the X chromosome is an active X chromosome. In addition, we also performed RNA FISH using an *XIST*-specific probe on the cell lines, because *XIST* is exclusively expressed from and remains associated with the inactive X

chromosome. We did not see any *XIST* signal in the RNA FISH analysis of OVCA680, ALST, CAOV3, and OVCA3 (data not shown). On the other hand, SKY and X chromosome painting analysis of SKOV3, one of the cell lines with relatively high levels of *XIST* expression, showed that there are five X chromosome in the cells (Fig. 3, *d* and *e*). RNA FISH with the *XIST*-specific probe demonstrated that this cell line is composed of cells with either one or two inactive X chromosome(s) (Fig. 3*f*). Hence, duplication of inactive X chromosome might contribute to the higher level of *XIST* expression in the SKOV3 cell line. Because both OVCA680 and CAOV3 contain only one X chromosome (Fig. 3*a* and data not shown), loss of inactive X chromosome may be one mechanism for the loss of *XIST* expression. In addition to loss of active X chromosome, some other mechanisms may be responsible for down-regulation of *XIST* expression. For example, some cell lines that exhibit low levels of *XIST* expression, such as OVCA3 and ALST, still maintain two X chromosomes (Fig. 3, *g* and *h*). There is an X chromosomal
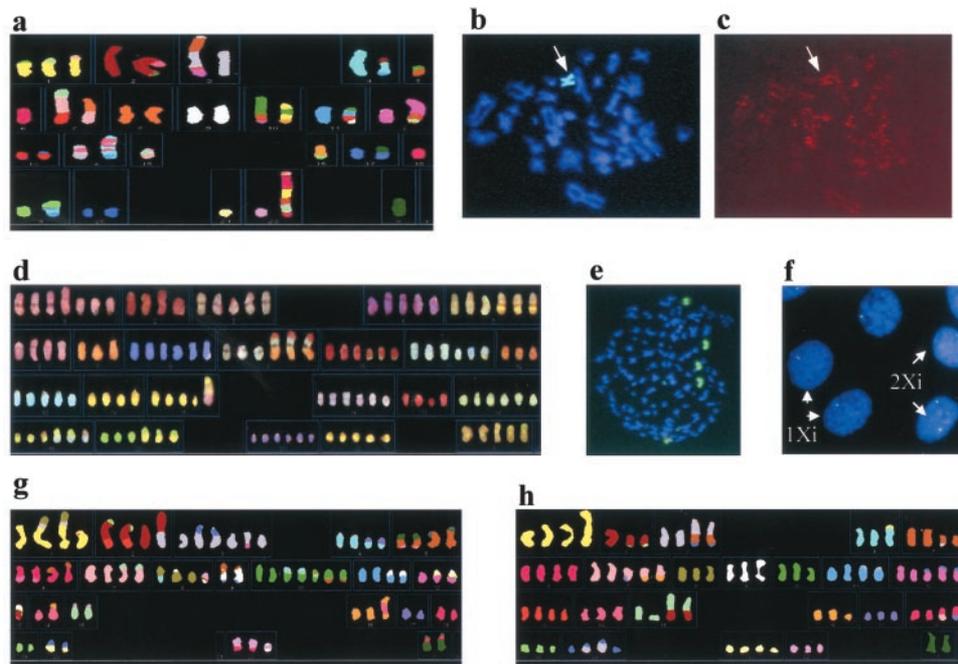
Fig. 3. SKY analysis and X chromosome status of ovarian cancer cell lines. *a,* SKY image of OVCA680 metaphase spread. Each color represents a unique spectral signature for a single chromosome. Chromosomes with multiple colors represent multiple chromosomal translocations that have been occurred. The single X chromosome is shown in *green* in the lower right corner. *b* and *c,* the same OVCA680 metaphase spread was double-stained for X chromosome (*green*) and acetylated histone H4 (*red*). *b,* the composite image of FITC-stained X chromosome and DAPI; *c,* the Texas Red staining for acetylated histone H4 (Lys-12) antibody. *Arrow,* position of X chromosome. *d,* SKY image of SKOV3 metaphase spread to show the five X chromosomes. *e,* X chromosome paint of SKOV3 metaphase spread. *f,* interphase RNA FISH with *XIST* transcript-specific probe on SKOV3 cells. The image is a composite image of the FITC-labeled *XIST* transcripts and DAPI-stained nuclei. *Arrows,* SKOV3 cells with either one or two inactive X chromosome(s). *g,* SKY image of OVCA3 metaphase spread. *h,* SKY image of ALST metaphase spread.

translocation observed in the OVCA3 cell line, whereas no obvious cytogenetic changes were identified in the ALST cells. These data suggest that multiple mechanisms might be involved in the changes of *XIST* expression in the ovarian carcinoma cell lines.

We then looked into the clinical relevance of *XIST* expression by analyzing patient responses to cancer chemotherapy. We chose primary tumor specimens from patients who have been treated with at least six cycles of carboplatin and Taxol after surgical cytoreduction and with medical history for at least 1 year after completion of chemotherapy. Two patients who were treated with triple-doublet protocol (three cycles of carboplatin/Taxol, two cycles of cisplatin/gemcitabine, and two cycles of Adriamycin/Topotecan) and relapsed within 6 months after completion of treatment were also included. All together, 21 cases collected from December 1995 to March 2000 were selected. Total RNAs were prepared from tumor tissues, and the *XIST* RNA levels were determined by quantitative real-time PCR. We chose relapse time (the time from completion of first-line chemotherapy to diagnosis of recurrent disease) as the parameter to measure the clinical outcome of the first-line chemotherapy. Correlation analysis was performed, and it was found that there was a strong correlation between relapse time and *XIST* expression level ($r = 0.653$, $P = 0.001$, $P_{boot} < 0.001$; Fig. 4). To account for other variables such as histology information, CA125, and patient age, as given in Table 2 multiple regres-
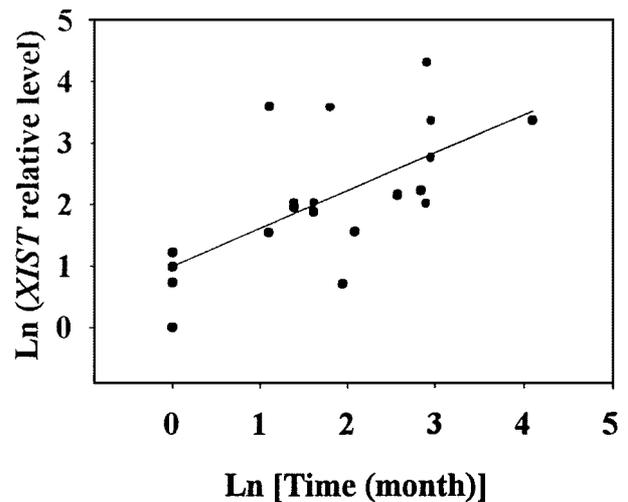
Fig. 4. Regression analysis of *XIST* RNA level and time of relapse.

sion analysis was also performed. We adopted the backwards elimination approach to select the predictor variables and chose the two-variable regression as the final model based on the sum of squares error and the degree of freedom. It was observed from the final model that *XIST* expression was significantly related to the relapse time and marginally to patient age (Table 3). For assessing the adequacy

Table 2   *XIST* expression and clinical outcome of ovarian cancer patients.

Time of relapse and other clinical information of the subjects as well as relative *XIST* RNA levels in the primary tumors. The relative *XIST* RNA levels and relapse times were log-transformed.

Patient ID	Ln(XIST)[a]	Ln(Time)[b]	Histology			Treatment	Age[c]	CA125[d]
			Subtype	Grade	Stage			
OV550	3.36	4.09	Serous	3	3	Carboplatin/Taxol	35	850
OV563	0.98	0.00	Serous	3	3C	Carboplatin/Taxol	64	1200
OV582	2.03	1.39	Serous	3	3C	Carboplatin/Taxol	38	6750
OV631	3.58	1.79	Serous	3	3C	Carboplatin/Taxol	67	1277
OV633	1.55	2.08	Serous	3	3C	Carboplatin/Taxol	70	3100
OV634	2.17	2.56	Serous	3	3C	Carboplatin/Taxol	43	42
OV635	1.21	0.00	Serous	3	3C	Carboplatin/Taxol	77	98
OV645	0.70	1.95	Serous	3	4	Carboplatin/Taxol	60	1370
OV650	1.87	1.61	Serous	3	3C	Carboplatin/Taxol	54	1330
OV652	0.73	0.00	Mucinous	1		Triple-Double[e]	58	73
OV657	1.95	1.39	Serous/Clear	3	4	Carboplatin/Taxol	57	119
OV688[f]	2.14	2.56	Endometriod	2	1A	Carboplatin/Taxol	54	68
OV689	2.22	2.83	Serous	3	3C	Carboplatin/Taxol	43	1100
OV690	3.59	1.10	Endometriod	3	4	Carboplatin/Taxol	36	1730
OV691	1.54	1.10	Serous	3	4	Carboplatin/Taxol	54	16000
OV694	2.03	1.61	Serous	3	3C	Carboplatin/Taxol	75	2157
OV700[f]	2.01	2.89	Mucinous	2	1A	Carboplatin/Taxol	78	20
OV715[f]	2.75	2.94	Serous	3	3C	Carboplatin/Taxol	61	Unknown
OV721	0.00	0.00	Serous	3	3C	Triple-Double[b]	57	2400
OV723[f]	3.36	2.94	Endometriod	2		Carboplatin/Taxol	53	Unknown
OV741[f]	4.30	2.89	Serous	3	2A	Carboplatin/Taxol	34	75

[a] *XIST* RNA level is presented as a natural logarithm of the expression level relative to that of OV721.
[b] Time of relapse, months after completion of chemotherapy.
[c] Patient's age when the disease was first diagnosed.
[d] Patient's preoperative serum CA125 value.
[e] Patient was treated with triple-doublet protocol (three cycles of carboplatin/Taxol, two cycles of cisplatin/gemcitabine, and two cycles of Adriamycin/topotecan).
[f] These patients still had not developed recurrent disease at time of the most recent visit.

Table 3   Multiple regression: final reduced model.

Variable	Regression coefficient		
	Estimate	Standard Error[a]	*P* value
Constant	6.482	3.067	0.049
Ln(Time)	0.512	0.165	0.006
Ln(Age)	−1.330	0.739	0.089

[a]Residual standard error: 0.803 (18 degree of freedom).

of the final model, residual plots were drawn, and they did not show any pattern, implying that the final model is adequate. Hence, significant positive correlation between *XIST* expression and relapse time still exists in the multivariate analysis.

Discussion

We explored the use of high-throughput cDNA microarray technology to identify potential prognostic markers for ovarian cancer by mRNA expression profiling of paired primary and recurrent tumors. Further studies of selected genes in ovarian carcinoma cell lines and patient samples have revealed a significant association of *XIST* expression level with Taxol sensitivity and chemotherapeutic responses. The high correlation of *XIST* RNA level and Taxol sensitivity in ovarian cancer cell lines suggests that *XIST* might play a role in modulating Taxol cytotoxicity. *XIST* is expressed exclusively from and remains associated with the inactive X chromosomes in female cells. Insertion of a 480-kb YAC genomic clone containing *XIST* gene to somatic chromosomes in mouse ES cells showed localized inactivation of adjacent genes on somatic chromosome as well as the neomycin marker gene on YAC vector (19). This suggests that *XIST* RNA can either directly or indirectly modulate the chromosome it associates with. As much about the molecular basis for *XIST* involvement in X chromosome inactivation is still lacking, it is also not known whether *XIST* has any possible direct effect on drug resistance other than X chromosome inactivation. Several attempts at reconstituting *XIST* expression in the ovarian cancer cell lines by transfection of YAC genomic DNA containing the *XIST* gene have failed, either because of low transfection efficiency or silencing of the *Neo* selection marker on YAC vector. Cotransfection with a second marker DNA and selection of clones for the presence of second marker may be an alternative approach.

One other plausible mechanism that *XIST* RNA modulates Taxol sensitivity is the reactivation of resistance-specific genes on inactive X chromosome in the absence of *XIST* RNA. Previous studies using the mouse/human somatic cell hybrids and human leukemia cells have shown that *XIST* RNA is not necessary for the maintenance of X inactivation once the cells are differentiated (20, 21). A more recent report suggested, however, the synergy of *XIST* RNA, DNA methylation, and histone hypoacetylation in maintaining the inactive state of X chromosome (22). Our RNA FISH study on SKOV3 cells showed punctuated *XIST* expression signals

localized to the *XIST* locus, unlike the intense signals covering the whole inactive X chromosome observed in differentiated mouse ES cells. More studies are under way to determine whether the situation is different in the differentiated ovarian cancer cell lines and whether the hypothesis that *XIST* modulates the expression of other genes is accountable for Taxol resistance, at least for those cells encompassing two or more X chromosomes. If it is true that *XIST* plays a role in regulating other resistance-specific gene(s) on the X chromosome, one possible down-stream candidate is XIAP, which is the most potent direct inhibitor of caspases and apoptosis among all human IAP family proteins (23). Down-regulated expression of *XIAP* has been shown to induce apoptosis in chemoresistant human ovarian cancer cells (24). Down-regulation of *XIST* might increase the expression level of XIAP and block drug-induced apoptosis to cause resistance phenotype.

It is also likely that loss of *XIST* expression is a marker for genetic instability associated with drug resistance, because loss of inactive X chromosome has been known to be a common event in cancer cells (25). However, the observed association between loss of *XIST* expression and drug resistance is only specific to Taxol, not to the alkylating agents (Fig. 1). The cell lines used in our study have not been pretreated with Taxol, and therefore the observed association is not attributable to drug-induced phenomenon. One possible explanation of this drug-specific association may lie with the action mechanism of Taxol. The action of Taxol is mediated through binding to microtubules and stabilizing them against depolymerization, thereby inhibiting cell replication by disrupting normal mitotic spindle formation (26). It has been observed that the action of Taxol on microtubules associates with mitotic arrest and induction of apoptosis, and mitotic arrest correlates with Taxol cytotoxicity (27). Treatments using Taxol together with other drugs that perturb cell cycle progression can dramatically interfere with the cell killing and apoptosis-inducing activity of Taxol (28). Mitotic checkpoint mechanisms regulated by MAD and BUB proteins control the proper segregation of chromosomes and play an important role in the genetic instability of cancers (29). It is therefore hypothesized that genetic instability in advanced cancer cells that have lost mitotic checkpoint function might cause the loss of *XIST* expression and the development of mechanism to escape Taxol-induced apoptosis as well.

In summary, our cDNA microarray analysis of paired primary and recurrent ovarian tumors has identified a high correlation between *XIST* RNA expression level and Taxol sensitivity in ovarian cancer cell lines. More interestingly, a strong correlation was also found between *XIST* RNA level and patient responses to chemotherapeutic treatment, suggesting that *XIST* expression might be used as a marker for prediction of first-line chemotherapy responses in ovarian cancer. This study raises an interesting perspective between X chromosome inactivation and drug resistance. Although the underlying mechanism for this correlation is unclear at present, more extensive studies on gene expression profiles of the paired primary and recurrent tumors may reveal more

insights into the relationship between these two apparently unrelated processes.

References

1. du Bois, A., Neijt, J. P., and Thigpen, J. T. First line chemotherapy with carboplatin plus paclitaxel in advanced ovarian cancer—a new standard of care? Ann. Oncol., *10:* 35–41, 1999.

2. Cannistra, S. A. Cancer of the ovary. N. Engl. J. Med., *329:* 1550–1559, 1993.

3. Ross, D. T., Scherf, U., Eisen, M. B., Perou, C. M., Rees, C., Spellman, P., Iyer, V., Jeffrey, S. S., Van de Rijn, M., Waltham, M., Pergamenschikov, A., Lee, J. C., Lashkari, D., Shalon, D., Myers, T. G., Weinstein, J. N., Botstein, D., and Brown, P. O. Systematic variation in gene expression patterns in human cancer cell lines. Nat. Genet., *24:* 227–235, 2000.

4. Scherf, U., Ross, D. T., Waltham, M., Smith, L. H., Lee, J. K., Tanabe, L., Kohn, K. W., Reinhold, W. C., Myers, T. G., Andrews, D. T., Scudiero, D. A., Eisen, M. B., Sausville, E. A., Pommier, Y., Botstein, D., Brown, P. O., and Weinstein, J. N. A gene expression database for the molecular pharmacology of cancer. Nat. Genet., *24:* 236–244, 2000.

5. van't Veer, L. J., Dai, H., van de Vijver, M. J., He, Y. D., Hart, A. A., Mao, M., Peterse, H. L., van der Kooy, K., Marton, M. J., Witteveen, A. T., Schreiber, G. J., Kerkhoven, R. M., Roberts, C., Linsley, P. S., Bernards, R., and Friend, S. H. Gene expression profiling predicts clinical outcome of breast cancer. Nature (Lond.), *415:* 530–636, 2002.

6. Singh, D., Febbo, P. G., Ross, K., Jackson, D. G., Manola, J., Ladd, C., Tamayo, P., Renshaw, A. A., D'Amico, A. V., Richie, J. P., Lander, E. S., Loda, M., Kantoff, P. W., Golub, T. R., and Sellers, W. R. Gene expression correlates of clinical prostate cancer behavior. Cancer Cell, *1:* 203–209, 2002.

7. Yeoh, E-J., Ross, M. E., Shurtleff, S. A., Williams, W. K., Patel, D., Mahfouz, R., Behm, F. G., Raimondi, S. C., Reilling, M. V., Patel, A., Cheng, C., Campana, D., Wilkins, D., Zhou, X., Li, J., Liu, H., Pui, C-H., Evans, W. E., Naeve, C., Wong, L., and Downing, J. R. Classification, subtype discovery, and prediction of outcome in pediatric acute lymphoblastic leukemia by gene expression profiling. Cancer Cell, *1:* 133–143, 2002.

8. Riggs, A. D., and Pfeifer, G. P. X-chromosome inactivation and cell memory. Trends Genet., *8:* 169–174, 1992.

9. Rastan, S., and Brown, S. D. The search for the mouse X-chromosome inactivation centre. Genet. Res., *56:* 99–106, 1990.

10. Heard, E., Clerc, P., and Avner, P. X-chromosome inactivation in mammals. Annu. Rev. Genet., *31:* 571–610, 1997.

11. Brown, C. J., Hendrich, B. D., Rupert, J. L., Lafreniere, R. G., Xing, Y., Lawrence, J., and Willard, H. F. The human *XIST* gene: analysis of a 17 kb inactive X-specific RNA that contains conserved repeats and is highly localized within the nucleus. Cell, *71:* 527–542, 1992.

12. Panning, B., Dausman, J., and Jaenisch, R. X chromosome inactivation is mediated by Xist RNA stabilization. Cell, *90:* 907–916, 1997.

13. Marahrens, Y., Panning, B., Dausman, J., Strauss, W., and Jaenisch, R. Xist-deficient mice are defective in dosage compensation but not spermatogenesis. Genes Dev., *11:* 156–166, 1997.

14. Penny, G. D., Kay, G. F., Sheardown, S. A., Rastan, S., and Brockdorff, N. Requirement for Xist in X chromosome inactivation. Nature (Lond.), *379:* 131–137, 1996.

15. Heard, E., Mongelard, F., Arnaud, D., Chureau, C., Vourc'h, C., and Avner, P. Human XIST yeast artificial chromosome transgenes show partial X inactivation center function in mouse embryonic stem cells. Proc. Natl. Acad. Sci. USA, *96:* 6841–6846, 1999.

16. Migeon, B. R., Luo, S., Stasiowski, B. A., Jani, M., Axelman, J., Van Dyke, D. L., Weiss, L., Jacobs, P. A., Yang-Feng, T. L., and Wiley, J. E. Deficient transcription of XIST from tiny ring X chromosomes in females

with severe phenotypes. Proc. Natl. Acad. Sci. USA, *90:* 12025–12029, 1993.

17. Efron, B. The Jackknife, the Bootstrap, and Other Resampling Plans, pp. 27–36. Philadelphia: SIAM, 1982.

18. Keohane, A. M., Barlow, A. L., Waters, J., Bourn, D., and Turner, B. M. H4 acetylation, XIST RNA and replication timing are coincident and define x;autosome boundaries in two abnormal X chromosomes. Hum. Mol. Genet., *8:* 377–383, 1999.

19. Migeon, B. R., Kazi, E., Haisley-Royster, C., Hu, J., Reeves, R., Call, L., Lawler, A., Moore, C. S., Morrison, H., and Jeppesen, P. Human X inactivation center induces random X chromosome inactivation in male transgenic mice. Genomics, *59:* 113–121, 1999.

20. Brown, C. J., and Willard, H. F. The human X-inactivation centre is not required for maintenance of X-chromosome inactivation. Nature (Lond.), *368:* 154–156, 1994.

21. Rack, K. A., Chelly, J., Gibbons, R. J., Rider, S., Benjamin, D., Lafreniere, R. G., Oscier, D., Hendriks, R. W., Craig, I. W., Willard, H. F., *et al.* Absence of the *XIST* gene from late-replicating isodicentric X chromosomes in leukaemia. Hum. Mol. Genet., *3:* 1053–1059, 1994.

22. Csankovszki, G., Nagy, A., and Jaenisch, R. Synergism of Xist RNA, DNA methylation, and histone hypoacetylation in maintaining X chromosome inactivation. J. Cell Biol., *153:* 773–784, 2001.

23. Deveraux, Q. L., and Reed, J. C. IAP family proteins—suppressors of apoptosis. Genes Dev., *13:* 239–252, 1999.

24. Sasaki, H., Sheng, Y., Kotsuji, F., and Tsang, B. K. Down-regulation of X-linked inhibitor of apoptosis protein induces apoptosis in chemoresistant human ovarian cancer cells. Cancer Res., *60:* 5659–5666, 2000.

25. Cheng, P. C., Gosewehr, J. A., Kim, T. M., Velicescu, M., Wan, M., Zheng, J., Felix, J. C., Cofer, K. F., Luo, P., Biela, B. H., Godorov, G., and Dubeau, L. Potential role of the inactivated X chromosome in ovarian epithelial tumor development. J. Natl. Cancer Inst., *88:* 510–518, 1996.

26. Schiff, P. B., and Horwitz, S. B. Taxol stabilizes microtubules in mouse fibroblast cells. Proc. Natl. Acad. Sci. USA, *77:* 1561–1565, 1980.

27. Blagosklonny, M. V., and Fojo, T. Molecular effects of paclitaxel: myths and reality (a critical review). Int. J. Cancer, *83:* 151–156, 1999.

28. Huang, T. S., Shu, C. H., Chao, Y., and Chen, L. T. Evaluation of GL331 in combination with paclitaxel: GL331's interference with paclitaxel-induced cell cycle perturbation and apoptosis. Anticancer Drugs, *12:* 259–266, 2001.

29. Chen, R. H., Waters, J. C., Salmon, E. D., and Murray, A. W. Association of spindle assembly checkpoint component XMAD2 with unattached kinetochores. Science (Wash. DC), *274:* 242–246, 1996.